Solid–gas interface thermal conductance for the thermal barrier coating with surface roughness: The confinement effect

Xue Zhao(赵雪)[1] and Jin-Wu Jiang(江进武)[1,2,†]

[1] *Shanghai Key Laboratory of Mechanics in Energy Engineering, Shanghai Institute of Applied Mathematics and Mechanics, School of Mechanics and Engineering Science, Shanghai University, Shanghai* 200072, *China*
[2] *Zhejiang Laboratory, Hangzhou* 311100, *China*

(Received 20 June 2022; revised manuscript received 10 August 2022; accepted manuscript online 8 September 2022)

The yttria-stabilized zirconia (YSZ) is a famous thermal barrier coating material to protect hot-end components of an engine. As a characteristic feature of the YSZ, the surface roughness shall play an important role in the interface thermal conductance between the YSZ and gas, considering that the gas is typically at an extremely high temperature. We investigate the effect of the surface roughness on the thermal conductance of the YSZ–gas interface with surface roughness described by nanoscale pores on the surface of the YSZ. We reveal two competitive mechanisms related to the microstructure of the pore, i.e., the actual contact area effect and the confinement effect. The increase of the pore depth will enlarge the actual contact area between the YSZ and gas, leading to enhancement of the solid–gas interface thermal conductance. In contrast to the positive actual contact area effect, the geometry-induced confinement effect greatly reduces the interface thermal conductance. These findings shall offer some fundamental understandings for the microscopic mechanisms of the YSZ–gas interface thermal conductance.

Keywords: interface thermal conductance, thermal barrier coating, solid–gas interface, confinement effect

PACS: 68.35.Ct, 44.10.+i, 81.05.Mh, 02.70.Ns **DOI:** 10.1088/1674-1056/ac9041

1. Introduction

Thermal barrier coating (TBC) is widely used in gas turbine engines.[1] TBC can reduce surface temperature of metal alloy substrates.[2] Higher operating temperature can increase the engine efficiency and extend the service time of the components.[3,4] There are two usual methods for spraying TBC on gas turbine components, i.e., air plasma spray (APS)[5] and electron beam physical vapor deposition (EB-PVD).[6] There are plenty of intercolumnar pore structures in TBC layers prepared by EB-PVD,[7] and this intercolumnar pore structure is perpendicular to the coating plane.[8,9]

This intercolumnar pore can influence the TBC interface. It is found that the elongated intercolumnar pore created by the EB-PVD enhances the flexibility of the coating on the substrate plane and improves the lifetime of the TBC.[7] Zhao *et al.* studied the effect of the pore volume fraction on the silicate melt infiltration in yttria-stabilized zirconia (YSZ) TBC.[10] Zhang *et al.* found that the infiltrated calcium magnesium aluminosilicate melt can solidify and occupy the internal space in the EB-PVD coated columnar, which causes significant deterioration in the strain tolerance and the insulation performance.[11] The pore's microstructure not only affects the mechanical properties but also has strong effects on the interface heat transfer of TBC.[12–14] The YSZ coating is usually exposed to high-temperature and high-pressure gases, so the heat transfer at the interface between the TBC and the hot gas is important.

Kapitza discovered the temperature jump at the interface between solid and liquid, resulting in the temperature discontinuity at the interface.[15] Chen *et al.* comparatively measured the heat transport of graphene monolayers suspended in vacuum and air by Raman experiments, and they obtained the interface thermal conductance between graphene and air.[16] Cheng *et al.* studied the heat loss rate at the nanowire-air interface by laser thermography and illustrated a general scaling relationship for gaseous heat dissipation from nanostructures.[17] The molecular dynamic (MD) simulation has been widely used to study the heat transfer of microstructures.[18–20] Markvoort *et al.* performed MD simulations to study the wetting effect on the heat transfer properties of the solid–gas interface.[21] Several works found that a better mass matching between the solid and gas can improve the efficiency of the heat exchange at the solid–gas interface.[22,23] Zhang *et al.* investigated the temperature jump at rough solid–gas interfaces, and the results show that the surface roughness is beneficial for the energy exchange at the solid–gas interface.[24] Some other effects on the solid–gas interface thermal conductance have also been studied, including the interface bonding strength[25,26] and the organic self-assembled monolayer.[27,28]

It has been proved that the porous structure of the YSZ has important effects on thermal conductivity of solid YSZ coating.[29] However, porous structure of the YSZ has limited effects on the interface thermal conductance between YSZ and gas, because the interface thermal conductance is domi-

†Corresponding author. E-mail: jiangjinwu@shu.edu.cn

© 2022 Chinese Physical Society and IOP Publishing Ltd

nated by the properties of the interface, especially the coupling strength between the solid and the gas.[28]

In this paper, we study the effect of surface roughness on the thermal conductance of the YSZ–gas interface, where the surface roughness is represented by rectangular pores. We focus on the pore's geometry effect on the interface thermal conductance. The interface thermal conductance is determined by two major effects: the actual contact area effect and the confinement effect. More specifically, the increase of the pore depth will increase the actual contact area of the interface between the YSZ and gas, resulting in the enhancement of the interface thermal conductance. In contrast, the geometry-induced confinement effect can greatly reduce the thermal conductance for the YSZ–gas interface with narrower pores.

2. Structure and simulation details

The schematic structure of the simulation model is shown in Fig. 1. We consider the zirconia stabilized by 8 wt% yttria. The lattice constants of the YSZ are $a = 7.187$ Å, $b = 12.448$ Å, and $c = 8.802$ Å. The size of the YSZ is denoted by three integers (n_x, n_y, n_z), which are the number of the unit cell along the x, y and z directions. The structure in our simulation has $(n_x, n_y, n_z) = (14, 2, 17)$. The similar size is used in the MD simulation for the heat transfer process across the solid–gas or solid-liquid interface.[22,30] Then the shape of the surface roughness can be sinusoidal function, triangle and rectangle.[31–33] To mimic the experimental sample,[34] we use a rectangular pore on the surface of the YSZ to represent the surface roughness. The pore is described by the depth d and the width w. Here the rectangular pore is used to mimic the roughness of the YSZ surface. The top of the YSZ is filled with gas molecules, which contain 80% N_2 and 20% O_2. The height of the gas region is 110 Å.

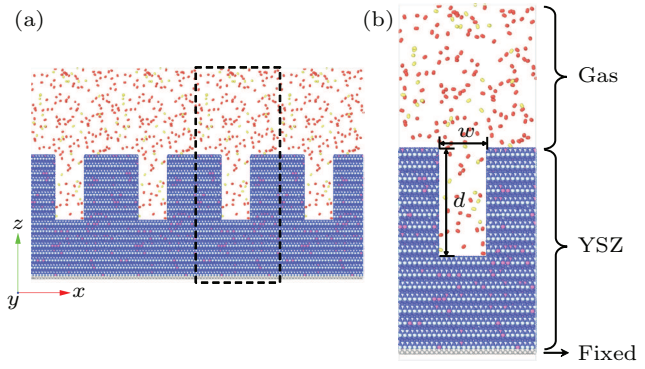


Fig. 1. Structure of the TBC-gas interface: (a) surface roughness of the TBC, (b) model for the molecular dynamics simulation.

The interaction within the YSZ is described by the following Buckingham potential:[35]

$$E(ij) = \frac{q_i q_j}{r_{ij}} + A_{ij}\exp\left(-\frac{r_{ij}}{\rho_{ij}}\right) - \frac{C_{ij}}{r_{ij}^6}, \tag{1}$$

which includes the Coulomb electrostatic interaction, the short-range repulsion between ions, and the long-range van der Waals interaction. Here, q_i and q_j are the charges of ions i and j, and r_{ij} is the distance between ions i and j. The potential parameters A_{ij}, ρ, and C_{ij} are listed in Table 1, which are from Ref. [36].

The intermolecular interaction of gas molecules in this paper is described by the 12–6 Lennard–Jones (LJ) potential

$$E_{\mathrm{vdW}}(r_{ij}) = 4\varepsilon\left[\left(\frac{\sigma}{r_{ij}}\right)^{12} - \left(\frac{\sigma}{r_{ij}}\right)^{6}\right], \tag{2}$$

where ε is the energy parameter, and σ is the length parameter. The values of ε and σ are obtained from the universal force field model.[37] The bonding between two atoms within a gas molecule is described by the harmonic bond potential

$$\phi_{\mathrm{v}}(x) = \frac{1}{2}K(x - x_{\mathrm{e}})^2, \tag{3}$$

where K is the force constant, and x_{e} is the equilibrium bond length of N_2 or O_2. The values of K and x_{e} are obtained from the universal force field model.[37] The potential parameters of the gas are listed in Table 2. The Lorentz–Berthelot combining rule is used to calculate the potential parameters for the interaction between elements.[38,39] The potential parameters of the interface between the YSZ and gas are listed in Table 3. The cutoff distance for all LJ interactions is 10 Å in this work.

Table 1. Buckingham potential parameters for YSZ.

	ρ (Å)	A (eV)	C (eV·Å^6)
O–O	0.224	9547.96	32.0
Zr–O	0.345	1502.11	5.1
Y–O	0.348	1366.35	19.6

Table 2. Potential parameters for nitrogen (N) and oxygen (O).

	ε (meV)	σ (nm)	K (eV/Å^2)	x_{e}
N–N	2.99	3.262	66.393	1.12
O–O	2.60	3.119	48.845	1.16
N–O	2.78	3.191		

Table 3. Lennard–Jones potential parameters for the YSZ–gas interface.

YSZ and gas (N and O)	ε (meV)	σ (nm)
Zr–N	2.99	3.023
Zr–O	2.78	2.952
O_{ZrO_2}–N	2.78	3.191
O_{ZrO_2}–O_{O_2}	2.60	3.119
Y–N	3.04	3.122
Y–O	2.86	3.051

The simulation is performed in two steps. Firstly, the solid is thermalized at 300 K within the NPT ensemble, while the gas is thermalized at 600 K within the NVT ensemble for 0.4 ns. The Nose–Hoover thermostat is used to realize constant temperature and pressure.[40,41] Secondly, the solid is allowed to evolve within the NVT ensemble at a constant temperature of 300 K. The gas evolves within the NVE ensemble

and the thermal energy of the gas will dissipate into the YSZ during the simulation. The temperature of the gas will decrease gradually. The time dependence of the gas temperature is recorded to extract the interface thermal conductance.

Periodic boundary conditions are used in MD simulations. The bottom region of the YSZ is fixed to avoid the shift of the solid during the simulation. All simulations are performed with LAMMPS,[42] and visualized by OVITO.[43] The equation of motion is integrated by the velocity Verlet algorithm with time steps of 1.0 fs.

3. Results and discussion

3.1. MD simulation results

The thermal conductance is calculated by the heat dissipation method.[44] The solid is set to a constant low temperature T_c. The high temperature of the gas (T_h) will decrease and approach to the solid's temperature, as a result of the heat dissipation process. According to Fourier's law and the definition of heat capacity, the gas temperature T_h is governed by[44]

$$C\rho d\frac{\partial T_h}{\partial t} = -G[T_h - T_c(0)], \tag{4}$$

where C is the specific heat capacity, ρ is the mass density, d is the thickness of solid, and G is the Kapitza conductance. From Eq. (4), the temperature difference between the solid and gas can be obtained as follows:

$$\Delta T(t) = \Delta T_0 \exp\left(-\frac{t}{\tau}\right), \tag{5}$$

where $\Delta T_0 = T_h(0) - T_c(0)$ is the initial temperature difference. The characteristic time τ is[44]

$$\tau = \frac{C_v}{A \cdot G}. \tag{6}$$

Here A is the interface area. The heat capacity of gas molecules is $C_v = \frac{f}{2}R$, with $R = 8.317$ J/(K·mol). The degree of freedom for the gas molecule is taken as $f = 5$ for the diatomic molecule.[45]

In this work, the characteristic time τ is obtained by fitting MD simulation results to Eq. (5). Then the interface thermal conductance is calculated from Eq. (6). Figure 2(a) shows the MD results of the time-dependent temperature for the gas and YSZ without pore defect. Figure 2(b) shows that the numerical results can be well fitted to the exponential function for the temperature difference. The structure of the YSZ has (n_x, n_y, n_z) = (41, 24, 3) in this figure. The height of the gas region is 100 Å. The fitted characteristic time is $\tau = 290.1$ ps. The resultant interface thermal conductance is 0.0161 MW/(m^2·K), which is comparable with the values of other solid–gas interfaces as listed in Table 4. We have used the gas density of 0.647 kg/m^3, which corresponds to the ambient pressure. To reduce the statistical error, we have repeated five independent MD simulations for each model. The averaged value is used as the predicted result. The maximum value of the error is less than 10%.

It should be noted that thermal radiation is an important factor for the thermal conductance, especially in a high temperature background.[46,47] In this work, we consider the contribution of the lattice heat transfer to the interface thermal conductance of the solid–gas interface.

Table 4. The value of the interface thermal conductance of the YSZ–gas interface compared with other solid–gas interfaces.

Interface	Thermal conductance [MW/(m^2 · K)]	Condition	Comment
YSZ–gas (this work)	0.0161	600 K and 1 bar	Simulation
Graphene–air[16]	$0.029 + 0.051/-0.029$	300 K and 1 bar	Experiment
Pt–Ar[25]	0.04	300 K and 1 bar	Simulation
Au–N_2[22]	0.52 ± 0.03	300 K and 10 bar	Simulation
Au–Ar[28]	0.76 ± 0.04	300 K and 15 bar	Simulation

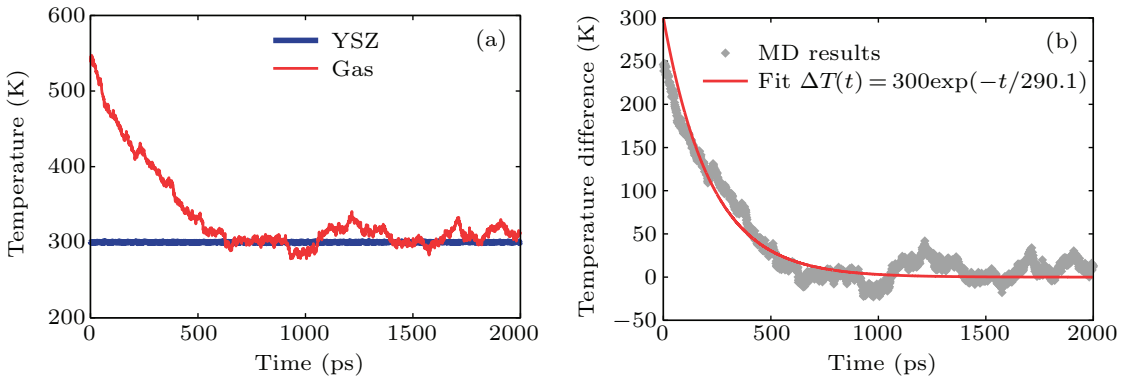


Fig. 2. The heat dissipation process: (a) the time-dependent temperature of the YSZ and gas, (b) the temperature difference between the YSZ and gas.

3.2. Initial temperature difference

We first study the effect of the initial temperature difference ΔT_0 on the thermal conductance of the YSZ–gas interface. For this set of simulations, the structure of the YSZ is $(n_x, n_y, n_z) = (27, 16, 2)$. The height of the gas region is 100 Å. The gas density is 233.390 kg/m^3. The initial temperature of the gas takes 400, 500, 600, 700 and 800 K. The relation between the initial temperature and the interface thermal conductance is shown in Fig. 3. The results indicate that the interface thermal conductance increases gradually with increasing initial temperature difference. Because the increase in temperature results in higher kinetic energy of gas molecules, the collision frequency between the gas molecules and the solid wall is increased, which can promote the heat exchange. Hence, the interface thermal conductivity is increased. The nonlinear scattering among gas molecules is also one possible reason for the initial temperature dependence of the interface thermal conductance. We thus choose a proper value of $\Delta T_0 = 300$ K in the following calculations.

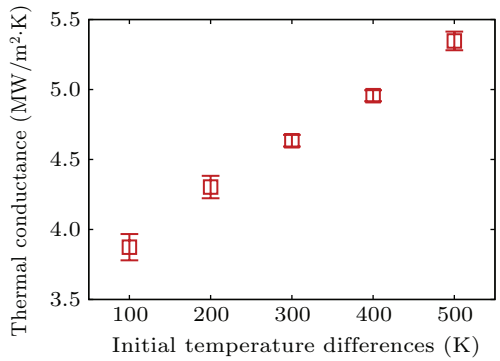


Fig. 3. The relation between the interface thermal conductance and the initial temperature differences.

3.3. Density effect

We study the effect of density on the interface thermal conductance of the YSZ–gas interface. For this set of MD simulations, we have $(n_x, n_y, n_z) = (27, 16, 2)$. The height of the gas region is 100 Å. The gas density takes 64.64, 129.29, 161.63, 193.93, and 233.39 kg/m^3. The value of the interface thermal conductance is shown in Fig. 4.

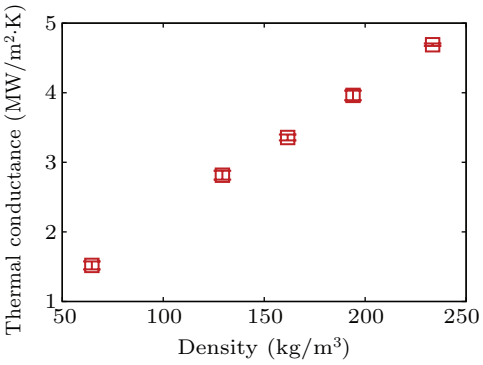


Fig. 4. The relation between the interface thermal conductance and the gas density.

We find that the interface thermal conductance increases with the increase of the gas density, because there are more gas molecules colliding with the YSZ surface for larger gas density, leading to stronger interface thermal transport. Furthermore, the collision among the gas molecules becomes stronger for larger gas density due to the nonlinear effect.

3.4. Effect of pore size

Figure 5(a) shows the thermal conductance of the YSZ–gas interface with pores of different depths. For this set of simulations, the depth of the pore is $d = N_d c$ with $N_d = 1$, 2, 3, 6, 9, 12, and 15. The widths of the pore is $w = N_w a$ with $N_w = 1$, 3, and 7. We note that a and c are the lattice constants as presented in the above section. The density of the gas is 233.511 kg/m^3 for these simulations. This density value is much larger than the gas density under the ambient condition, which saves the simulation cost.

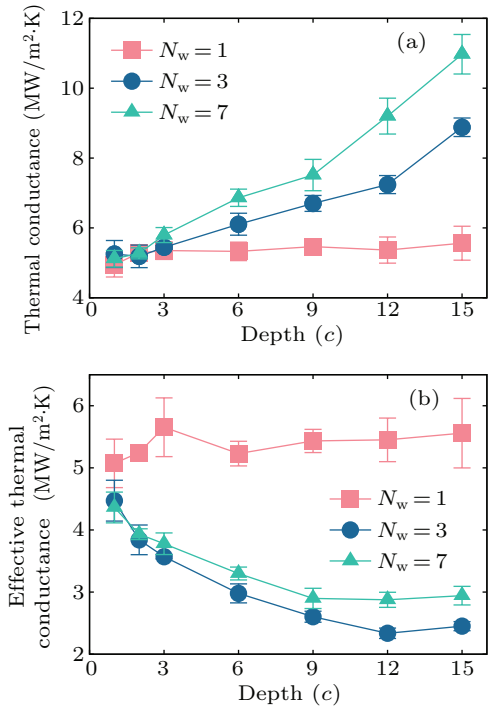


Fig. 5. The depth dependence for (a) the thermal conductance and (b) the effective thermal conductance.

It can be seen from Fig. 5(a) that the interface thermal conductance increases with increasing pore depth for a given pore width. This is because the actual contact area between the YSZ and gas is enhanced by the increase of the pore depth, which promotes the heat exchange between the YSZ and gas. To further understand this area enhancement effect, we can define an effective thermal conductance, $G' = (\frac{n_x a}{n_x a + 2d})G$, which excludes the area enhancement effect. Here we have $n_x = 14$. The effective thermal conductance is shown in Fig. 5(b). For the large pore with $N_w = 3$ and 7, the effective thermal conductance should be a constant as the area enhancement effect is excluded in G'. However, the effective thermal conductance decreases with increasing pore depth, which may be due to

other mechanisms. We will further explore this new mechanism in the next section. It should be noted that for the extremely narrow pore with $N_w = 1$, the area enhancement effect does not play a role. Because the pore is so narrow that only few gas molecules can diffuse into the pore, the inner surface of the pore does not contribute to the heat dissipation process.

Figure 6 shows the interface thermal conductance of the YSZ–gas interface of different pore widths. For this set of simulations, the width is $w = N_w a$ with $N_w = 1$, 2, 3, 5, 7, and 10. The depth is $d = N_d c$ with $N_d = 2$, 9, and 15. We find that the interface thermal conductance remains almost unchanged with increasing width when the depth is a small value of $N_d = 2$. This is because the actual contact area keeps the same for the surface with different pore depths. However, for larger pore depth of $N_d = 9$ and 15, the interface thermal conductance increases considerably with the increase of the pore width, though the actual contact area is not changed. This is due to the confinement effect, which is discussed in the next section.

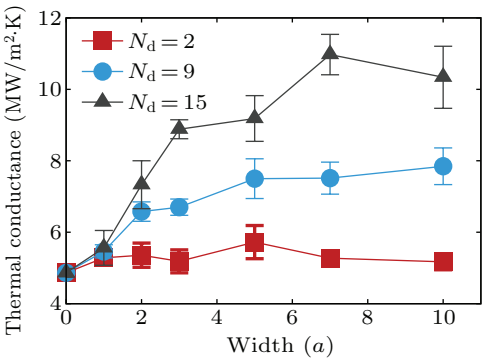


Fig. 6. Effect of the pore width on the interface thermal conductance.

3.5. Confinement effect

From the above discussions, we have understood that the interface thermal conductance can be enhanced by increasing the actual contact area, especially for larger pore depths. However, we have also found that the interface thermal conductance can be affected by different pore widths, although the actual contact area is the same for pores with different widths. Besides the actual contact area effect, the geometry-induced confinement effect is also important for the heat dissipation through the interface between the solid and gas.

To explain the confinement effect, we monitor the motion of the gas molecules inside the pore. At time $t = 0$, all molecules in the pore are marked. These marked molecules will exchange with other molecules outside the pore, so the ratio of the marked molecules inside the pore will decrease with time evolution. Figure 7(a) shows the time dependence for the ratio of the marked molecules, which decreases gradually with time. The decrease of the ratio is slower for narrower pores, because the gas molecules in narrower pores are more difficult to exchange with external molecules. This is a direct result from the confinement effect. The time history of the ratio of the marked molecules can be fitted to the exponential function $y = c_1 + c_2 \exp(-t/\tau_{con})$, with c_1, c_2, and τ_{con} as fitting parameters. The parameter τ_{con} is the characteristic time for the confinement effect, which represents the typical time for the gas molecule to stay in the pore. A larger value of τ_{con} indicates that the gas molecule is confined in the pore for a longer time, which means that the confinement effect is stronger. Figure 7(b) shows that the confinement time is larger for pores with smaller widths. The confinement time is also sensitive to the pore depth. We thus introduce the width to depth ratio, $\gamma = w/d$, to estimate the degree of confinement for the pore. Figure 7(c) shows that the confinement time decreases exponentially with the structural ratio γ.

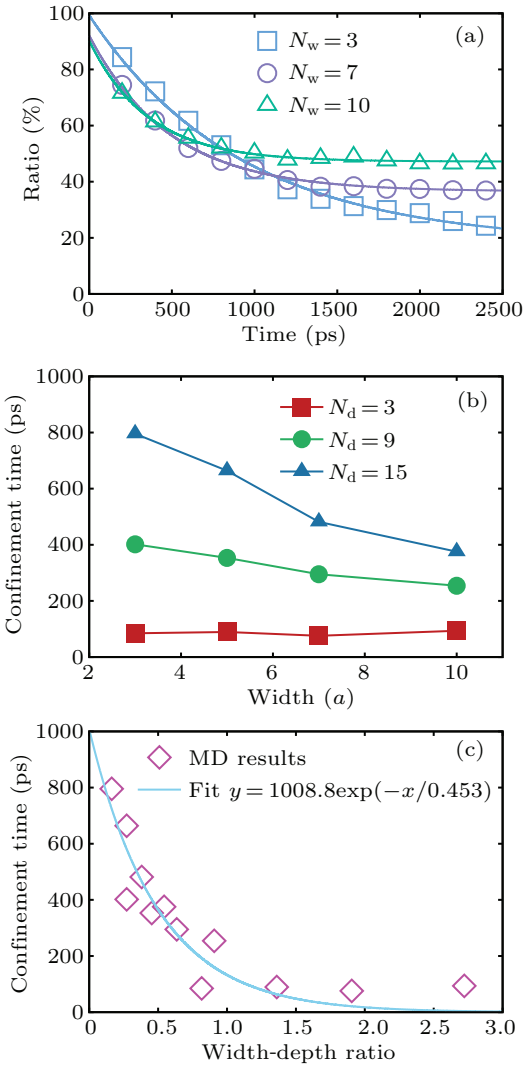


Fig. 7. Confinement effect on the interface thermal conductance: (a) time dependence for the ratio of the marked gas molecules left inside the pore, (b) the pore width dependence for the confinement characteristic time, (c) the confinement characteristic time versus the width-to-depth ratio.

A longer confinement time implies that the gas molecules confined in the pore exchange their thermal energy with external molecules more slowly. As a result, the inner surface of the

pore makes less contribution to the heat dissipation process. This is the origin for the reduction of the interface thermal conductance by the confinement effect. According to Fig. 7(c), the interface thermal conductance is larger for the pore with a larger structural ratio γ.

As a result of the confinement effect, the temperature is not uniform for the molecules confined inside the pore. To describe this temperature nonuniform phenomenon, we divide the pore into the top region and the bottom region, and calculate the temperature for these two regions. Figure 8 shows that the temperature of the top region is obviously higher than that of the bottom region, which further confirms the above confinement effect.

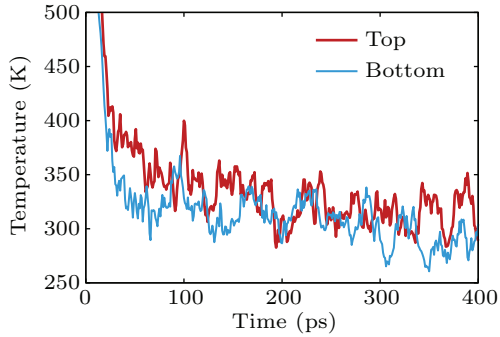


Fig. 8. Temperature for the top and bottom regions inside the pore.

4. Conclusions

In summary, we have studied the heat transfer on the YSZ–gas interface with the heat dissipation method by MD simulations. We examine the effect of the microstructure of the pore at the interface on the interface thermal conductance. It is found that the interface thermal conductance increases gradually with increasing initial temperature difference and gas density. We explore two important mechanisms for the interface thermal conductance: (i) The increase of the actual contact area at the YSZ–gas interface can enhance the interface thermal conductance. As a result, the interface with a pore of larger depth has larger interface thermal conductance, while the pore width is less important. (ii) The geometry-induced confinement effect will greatly reduce the interface thermal conductance. We disclose that the confinement strength decreases exponentially with the width-to-depth ratio of the pore.

Acknowledgements

Project supported by the National Natural Science Foundation of China (Grant Nos. 11822206 and 12072182), the Innovation Program of the Shanghai Municipal Education Commission (Grant No. 2017-01-07-00-09-E00019), the Key Research Project of Zhejiang Laboratory, and the National Supercomputing Center in Zhengzhou (Grant No. 2021PE0AC02).

References

[1] Guo S, Tanaka Y and Kagawa Y 2007 *J. Eur. Ceram. Soc.* **27** 3425
[2] Padture N P, Gell M and Jordan E H 2002 *Science* **296** 280
[3] Clarke D R, Oechsner M and Padture N P 2012 *MRS Bull.* **37** 891
[4] Wang L, Zhong X, Zhao Y, Yang J, Tao S, Zhang W, Wang Y and Sun X 2014 *Int. J. Heat Mass Transfer* **79** 954
[5] Koolloos M, Van Liempd G and Houben J 1998 *Surf. Eng.* **14** 144
[6] Unal O, Mitchell T E and Heuer A H 1994 *J. Am. Ceram. Soc.* **77** 984
[7] Hass D, Slifka A J and Wadley H 2001 *Acta Mater.* **49** 973
[8] Strangman T E 1985 *Thin Solid Films* **127** 93
[9] Schulz U, Oettel H and Bunk W 1996 *Int. J. Mater. Res.* **87** 488
[10] Zhao H, Levi C G and Wadley H N 2014 *Surf. Coat. Technol.* **251** 74
[11] Zhang G, Fan X, Xu R, Su L and Wang T 2018 *Ceram. Int.* **44** 12655
[12] Litovskii E Y 1972 *J. Eng. Phys.* **22** 768
[13] Nicholls J R, Lawson K, Johnstone A and Rickerby D 2002 *Surf. Coat. Technol.* **151** 383
[14] Renteria A F, Saruhan B, Schulz U, Raetzer-Scheibe H J, Haug J and Wiedenmann A 2006 *Surf. Coat. Technol.* **201** 2611
[15] Kapitza P 1941 *Phys. Rev.* **60** 354
[16] Chen S, Moore A L, Cai W, Suk J W, An J, Mishra C, Amos C, Magnuson C W, Kang J, Shi L and Ruoff R S 2011 *ACS Nano* **5** 321
[17] Cheng C, Fan W, Cao J, Ryu S G, Ji J, Grigoropoulos C P and Wu J 2011 *ACS Nano* **5** 10102
[18] Wang S, Xu J L and Zhang L Y 2017 *Acta Phys. Sin.* **67** 204704 (in Chinese)
[19] Wang T Y, Zhang G X and Li D Y 2021 *Chin. Phys. B* **30** 128101
[20] Hu S, Zhao C Y and Gu X 2022 *Chin. Phys. B* **31** 056301
[21] Markvoort A J, Hilbers P and Nedea S 2005 *Phys. Rev. E* **71** 066702
[22] Liang Z and Keblinski P 2014 *Int. J. Heat Mass Transfer* **78** 161
[23] Rabani R, Heidarinejad G, Harting J and Shirani E 2020 *Int. J. Therm. Sci.* **153** 106394
[24] Zhang C, Deng Z and Chen Y 2014 *Int. J. Heat Mass Transfer* **70** 322
[25] Liang Z, Evans W and Keblinski P 2013 *Phys. Rev. E* **87** 022119
[26] Giri A, Braun J L and Hopkins P E 2016 *J. Phys. Chem. C* **120** 24847
[27] Day B S and Morris J R 2005 *J. Chem. Phys.* **122** 234714
[28] Liang Z, Evans W, Desai T and Keblinski P 2013 *Appl. Phys. Lett.* **102** 061907
[29] Zhao S, Shao C, Zahiri S, Zhao C and Bao H 2018 *J. Shanghai Jiaotong Univ. (Sci.)* **23** 38
[30] Lin T, Li X and Cheng P 2018 *Int. J. Heat Mass Transfer* **97** 118
[31] Song Z, Cui Z, Cao Q, Liu Y and Li J 2021 *J. Mol. Liq.* **337** 116052
[32] Cao B Y, Chen M and Guo Z Y 2004 *Chin. Phys. Lett.* **21** 1777
[33] Mei T, Chen Z X, Yang L, Wang K and Miao R C 2019 *Acta Phys. Sin.* **68** 094701 (in Chinese)
[34] Hass D, Slifka A J and Wadley H 2001 *Acta Mater.* **49** 973
[35] Buckingham R A 1938 *Proc. R. Soc. London A* **168** 264
[36] Schelling P K, Phillpot S R and Wolf D 2001 *J. Am. Ceram. Soc.* **84** 1609
[37] Rappé A K, Casewit C J, Colwell K, Goddard III W A and Skiff W M 1992 *J. Am. Ceram. Soc.* **114** 10024
[38] Lorentz H A 1881 *Ann. Phys. (Berlin)* **248** 127
[39] Berthelot D 1898 *Comptes Rendus Hebdomadaires des Séances de L'Académie des Sciences* **126** 1703
[40] Nosé S 1984 *J. Chem. Phys.* **81** 511
[41] Hoover W G 1985 *Phys. Rev. A* **31** 1695
[42] Plimpton S 1995 *J. Comput. Phys.* **117** 1
[43] Stukowski A 2009 *Model. Simul. Mater. Sci. Eng.* **18** 015012
[44] Stoner R and Maris H 1993 *Phys. Rev. B* **48** 16373
[45] Bond J W, Watson K M, Welch J A and Fu X L 1965 *Atomic Theory of Gas Dynamics* (Beijing: Science Press) pp. 10–15 (in Chinese)
[46] Zhang B J, Wang B X and Zhao C Y 2014 *Int. J. Heat Mass Transfer* **73** 59
[47] Bao H, Yan C, Wang B, Fang X, Zhao C Y and Ruan X 2017 *Sol. Energ. Mater. Sol. Cells* **168** 78